Cement and Concrete Composites 84 (2017) 188–197

Contents lists available at ScienceDirect

Cement and Concrete Composites

journal homepage: www.elsevier.com/locate/cemconcomp

Time-dependent characterization of Na_2CO_3 activated slag

B. Yuan, Q.L. Yu*, H.J.H. Brouwers

Department of the Built Environment, Eindhoven University of Technology, P.O. Box 513, 5600 MB Eindhoven, The Netherlands

ARTICLE INFO

Article history:
Received 1 June 2015
Received in revised form
21 March 2017
Accepted 5 September 2017
Available online 13 September 2017

Keywords:
Na_2CO_3 activation
Isothermal calorimetry
Reaction kinetics
Reaction products
Microstructure
Compressive strength

ABSTRACT

This study aims to investigate the time-dependent characteristics of sodium carbonate activated slag at the early stage and its compressive strength development. The reaction kinetics of Na_2CO_3 activated slag is analyzed at the curing ages of 1h, 6h, 1d, 2d, 3d, 4d and 7d, respectively, and the reaction products are characterized employing FTIR, XRD, TG-DTG and SEM. The results show that a weak reflection of gaylussite is observed after 1 d of curing, while intensive accumulation of gaylussite and formation of hydrotalcite are observed at 2 d/3 d. Meanwhile, the gelation of C-(A)–S–H after 3 d of curing is identified by FTIR. The role of pH, CO_3^{2-} anion concentration and the formation of crystals such as gaylussite and hydrotalcite on the reaction process are discussed. In addition, a relationship between the initial alkali concentration and compressive strength at different curing ages of 7 d, 28 d and 180 d is derived.

1. Introduction

Great attention has been paid to the increased environmental concerns in recent years, and measures such as to reduce the usage of conventional cement based materials and to recycle industrial wastes have been investigated. It is widely considered that alkali activated materials (AAM) could be one of the promising alternatives to the currently used cement, considering both mechanical properties, durability and applications [1–4]. Ground granulated blast furnace slag (GGBFS), one of the most applied raw materials in AAM, and its blends with supplementary materials have been extensively studied [5–7]. The alkali activation of slag involves the dissolution of calcium and aluminium to form a C-(A)–S–H type gel [5,8], promoting the generation of final product with high strength and good durability [9–11].

Up to date, the effect of alkali activators, concentrations and compound alkali activators on the mechanical properties of AAM has been extensively studied. Wang et al. [12] reported that waterglass is the best activator and the optimal alkali dosage (Na_2O.wt.%) is within the range of 3.0–5.5% by mass of slag. Bakharev et al. [13] concluded that liquid sodium silicate produces the highest mechanical strength, followed by sodium carbonate (Na_2CO_3, optimum proportion 4% Na). Although sodium silicate as an alkali activator shows numerous advantages in AAS, problems such as fast setting is often reported [8,14–16]. Zivica [17] studied the influence of alkali type and temperature (20–31 °C) on the setting of waterglass activated slag with a Na_2O content of 5 wt% and reported that the initial setting time of sodium silicate activated slag paste is significantly shortened from 40 min to 0 min when the temperature increases from 20 °C to 23 °C. According to Jimenez and Puertas [18], the fast setting of sodium silicate activated slag is attributed to the formation of an initial calcium silicate hydrate, while the initial formation of calcium carbonate is responsible for the retarded reaction process of Na_2CO_3 activated slag. On the other hand, high shrinkage of slag activated by sodium silicate solution was also extensively reported [19–22]. Collins et al. [19,20] investigated the cracking tendency and micro-cracking of alkali activated slag concrete and reported that its shrinkage was about two times larger than ordinary Portland cement (OPC) produced concrete. Cengiz et al. [21] reported that Na_2CO_3 activated slag have a similar or lower shrinkage than PC mortar, while slag activated by waterglass generally shows 3–6 times higher than that of PC mortar.

By far, only the reaction of sodium silicate and sodium hydroxide activated slag has been systematically addressed. Although sodium carbonate as an alkali activator has shown great potential in alkali activated system and has a superiority in terms of shrinkage, its reaction mechanism and activation effect is still not clearly understood. It is reported that a delayed reaction of slags activated by sodium carbonate is caused by the initial formation of calcium

* Corresponding author.
E-mail address: q.yu@bwk.tue.nl (Q.L. Yu).

https://doi.org/10.1016/j.cemconcomp.2017.09.005
0958-9465/

carbonate and mixed sodium/calcium carbonate double salts, as explained by Jimenez and Puertas [18]. Furthermore, a reaction mechanism of sodium/potassium carbonate activated slags was proposed by Xu and Provis [23] after examining the specimens cast between 1964 and 1982, considering that M_2CO_3 (M = Na, K) maintains a buffered alkaline environment for the ongoing reaction. However, the reaction products of sodium carbonate at the early age remain unclear. More specifically, the time when the hardening process of sodium carbonate starts is not yet clear.

As a matter of fact, carbonate anions are the main component of the pore solution of aged samples, even the activator applied is not sodium carbonate [24,25]. When characterizing the reaction products of carbonated sodium silicate activated slag, Bernal et al. [24] observed the formation of different hydrous sodium carbonate in the pore solution depending on the carbonation condition such as CO_2 partial pressure, temperature and relative humidity. Meanwhile, a recent research on the characterization of naturally carbonated alkali activated slag concretes shows that after a long period exposed to atmosphere, calcite, vaterite, and natron are identified as the main carbonation products [25]. It is obvious that carbonate anions play an important role on the strength development of aged alkali activated slag. As a result, a deeper understanding of sodium carbonate especially at the early age is of great interest. However, up till now, investigations on the early age behavior of sodium carbonate activated slag are limited and most researches only claim that the initial precipitation of $CaCO_3$ is responsible for the delayed reaction process.

This study investigates the reaction kinetics of sodium carbonate activated GGBFS at the early stage. The reaction process is measured by an isothermal calorimeter and the reaction products at different ages, based on the reaction kinetics results, are further characterized by Fourier transform infrared spectroscopy (FTIR), X-ray diffractometry (XRD), and thermogravimetric and derivative thermogravimetic analyses (TG-DTG). Moreover, the strength development of samples with different recipes at different curing ages were studied and the influential factors, including alkali dosage, water to solid ratio and curing age, are evaluated. Furthermore, the mechanism for the restarted reaction process after a lengthened dormant period is discussed.

2. Materials and experiments

2.1. Materials

The ground granulated blast furnace slag (GGBFS) used in this study was provided by ENCI B.V., the Netherlands, with a Blaine surface area of 300 m^2/kg. Table 1 presents the chemical composition of the GGBFS, determined by X-ray Fluorescence (XRF). The particle size distribution (PSD) was determined by laser granulometry (Mastersizer 2000) with the d(0.5) of 19.18 μm, as shown in Fig. 1.

The investigated alkali activator was sodium carbonate (powder form, analytical grade). The powder of alkali activator was firstly dissolved in water and followed by cooling down to room temperature (20 ± 1 °C) prior to further use. Recipes with different contents of alkali activator and different amounts of water were designed, as shown in Table 2.

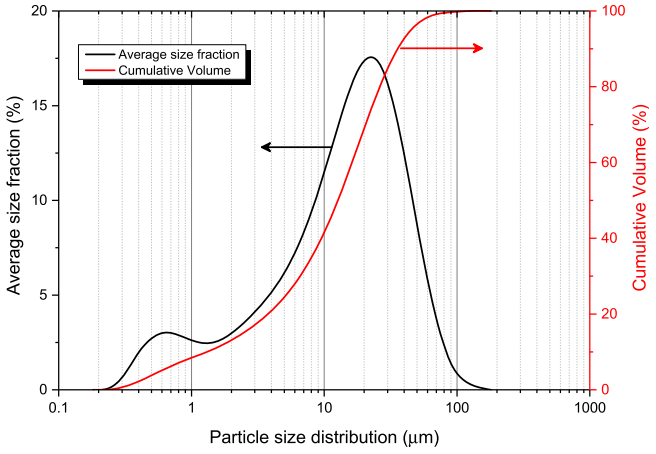

Fig. 1. Particle size distribution of GGBFS.

Table 2
Mix proportions of GGBFS activated by Na_2CO_3.

Mixture No.	Na_2CO_3 content (Na_2O wt.%)	W/S ratio	Mass/g		
			Na_2CO_3	GGBFS	Water
1	5	0.50	307.80	3600	1953.90
2		0.45	307.80		1758.51
3		0.40	307.80		1563.12
4	4	0.50	246.24		1923.12
5		0.45	246.24		1730.81
6		0.40	246.24		1538.50
7	3	0.50	184.68		1892.34
8		0.45	184.68		1703.11
9		0.40	184.68		1513.87

2.2. Experimental program

The reaction heat released from the slag reacted with alkali activators was analyzed by an isothermal calorimetry instrument (TAM AIR Calorimeter). The materials were first mixed and then transferred to an ampoule that is then loaded to the calorimeter. In general, the preparation would take 4–5 min before the measurement can start (i.e. this period cannot be analyzed). The temperature of the instrument is set to 20 °C and the calorimetry data were normalized by the amount of solids added to the mixture, including the mass of slag and sodium carbonate.

The fresh samples were prepared by mixing the solid materials and the designed activators (Table 2). Specimens for compressive strength test were cast with the size of 40 × 40 × 160 mm^3 in plastic moulds, following EN 196-1. The specimens were manually vibrated and then sealed with plastic foils to prevent the moisture loss. Most of specimens could not be demoulded after 2 d of casting because of the slow reaction rate. In this case, the samples were removed from the moulds after 3 d of curing (room temperature, 20 ± 1 °C) and then cured in water at room temperature until the testing age for the strength determination, while the samples for the early age behavior analysis were directly taken from the moulds at relevant curing times.

The FTIR analysis was firstly carried out to the selected samples

Table 1
Chemical composition of GGBFS determined by XRF.

Components	CaO	SiO_2	Al_2O_3	Fe_2O_3	K_2O	Na_2O	S-total	MgO	TiO_2	Cl	LOI
Content (wt.%)	36.97	34.02	13.03	0.46	0.46	0.34	1.22	9.78	0.97	0.01	2.70

after 28 d of curing. Afterwards, mixture M3 with the highest reaction rate studied here, which will be discussed in Section 3.1, was selected for further characterization. Based on the calorimetry analysis (see the identification in Fig. 2b), the samples of mixture M3 at different curing ages (1 h, 6 h, 1 d, 2 d, 3 d, 4 d and 7 d) were collected for further analysis (Fig. 2), applying FTIR, XRD, TGA-DTG and SEM. The samples were firstly ground into powders (≈63 μm) in the ethanol solution (absolute, 99.99%) and then washed by the ethanol solution for three times and then put in the oven to dry for 3 h at the temperature of 40 °C. In general, samples before 2 d after casting were easily dispersed and separated into fine particles in the ethanol solution, while samples from 3 d after casting needed to be ground because of the hardened condition. The samples at 28 d for the FTIR analysis were taken from the crushed specimens after the compressive strength test.

The FTIR spectra for the reaction products were collected using a Varian 3100 FTIR Spectrometer. All spectra were obtained with 48 scans per spectrum. Using a Cu tube (20 kV, 10 mA) with a scanning range from 5° to 55° 2θ, the reaction products were qualitatively analyzed by X-ray diffractometry (XRD, Bruker D5000), applying a step of 0.02° and 3 s/step measuring time. Furthermore, the reaction product was analyzed by thermogravimetric and derived thermogravimetric analyses (TG-DTG) at the heating rate of 1 °C min^{-1} from 20 °C to 1000 °C using a platinum holder. The scanning electron microscopy (SEM) was applied to study the microstructure development of samples at different curing ages.

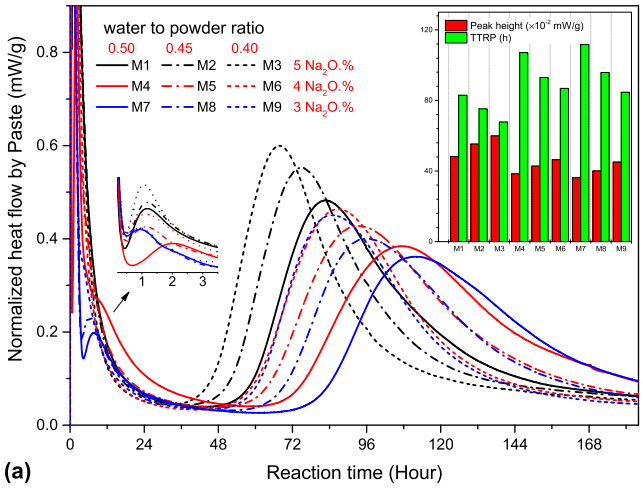

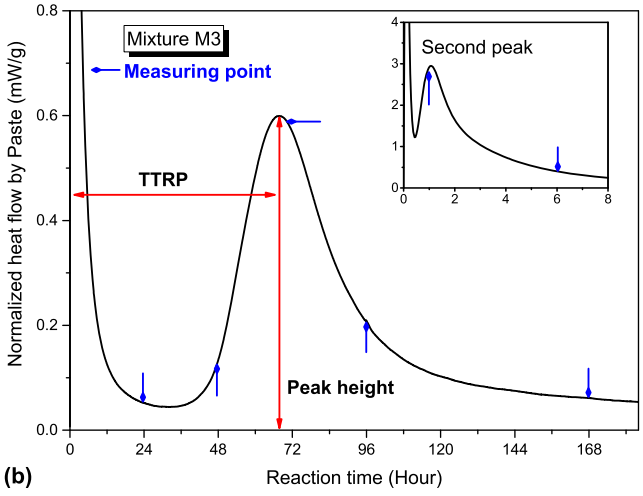

Fig. 2. Heat release of the designed sodium carbonate activated slags at 20 °C measured by isothermal calorimeter.

3. Results and discussion

3.1. Isothermal calorimetry

Fig. 2 shows the heat release of the samples with different sodium carbonate dosages and water-to-solid ratios. As can be seen, the reaction process can be generally classified into five stages, which is similar to that of waterglass activation or cement hydration [8,14,26]. However, sodium carbonate activation presents a prolonged dormant period and the time to reach the reaction peak (TTRP) of the investigated mixture ranges from 67 h to 112 h. Bernal et al. [27] reported a TTRP of ≈130 h with a water/binder ratio of 0.40 and an activator (Na_2CO_3) content of 8 wt%. In previous research, the authors reported that the fineness of slags has a significant role on the reaction rate of sodium carbonate activated slag [28], and Bernal et al. [29] concluded that the MgO content of slag significantly influences the reaction kinetics of alkali activated slag binders. In this case, the main differences on the reaction kinetics between the current study and previous reports could be attributed to the different fineness and chemistry of the slags applied.

It is clear that increasing the sodium carbonate dosage or lowering the water-to-solid ratio also slightly accelerate the reaction (Fig. 2). Shi and Day [30] studied the early age (up to 48 h) reaction kinetics of slag activated by different types of alkaline solutions at different temperatures (25 °C and 50 °C), including NaOH, $Na_2SiO_3 \cdot 5H_2O$, Na_2CO_3, Na_3PO_4, Na_2HPO_4 and NaF. They concluded that the initial pH is a key factor on the initial reaction rate but the further reaction is dominated by the Ca-compounds. By using calcined layered double hydroxides (CLDH), Ke et al. [31] observed that the reaction of sodium carbonate activated slag was accelerated because CLDH removed CO_3^{2-} anion from fresh sample, yielding a significant rise in the pH. In this case, the slight acceleration on the reaction can be attributed to the potentially high pH rising after dosing more alkalis with a lower water content.

As for waterglass activated slag, the heat evolution can be significantly affected by the Na_2O-to-slag ratio and activator modulus (M_s) [32]. Within the range of 5%–15% (Na_2O) and 1.0–2.0 (M_s), the time to reach the reaction peak ranges from 1 h to 30 h, which is clearly different from sodium carbonate activated slag (67 h–112 h). On the other hand, slag activated by sodium hydroxide does not show a clear induction period [30,32]. It is obvious that the reaction process of sodium carbonated slag, compared to other activators activated slag, is different, by possessing a long period of dormant period and showing another precipitation peak (Fig. 2a). To further characterize the reaction process of sodium carbonate activated slag, mixture M3 was selected and the reaction products were identified at different curing ages as shown in Fig. 2b. A more detailed analysis and discussion will be presented in the following sections.

3.2. FTIR

Fig. 4a shows the FTIR spectra of some selected samples. The results show that though with different proportions, the reaction products remain similar, mainly containing free water, CO_3^{2-} anions and C-(A)–S–H gel. In this case, sample mixture M3 with the highest reaction rate at the early age (Fig. 2b), which was selected for further analysis, can generally represent the reaction process of sodium carbonate activated slag. The pictures of the collected samples from mixture M3 are shown in Fig. 3. It can be seen that along with the reaction time, the colour of samples is gradually changing to green, indicating the ongoing reaction process.

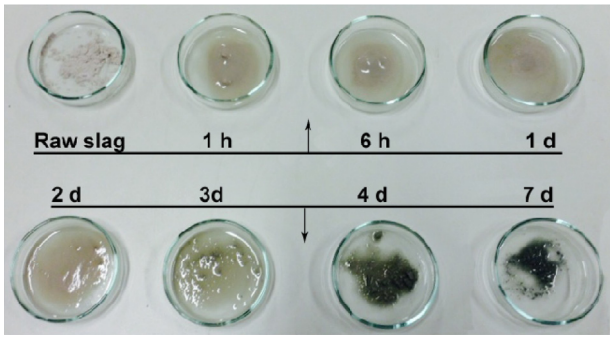

Fig. 3. Pictures of mixture M3 at different curing ages.

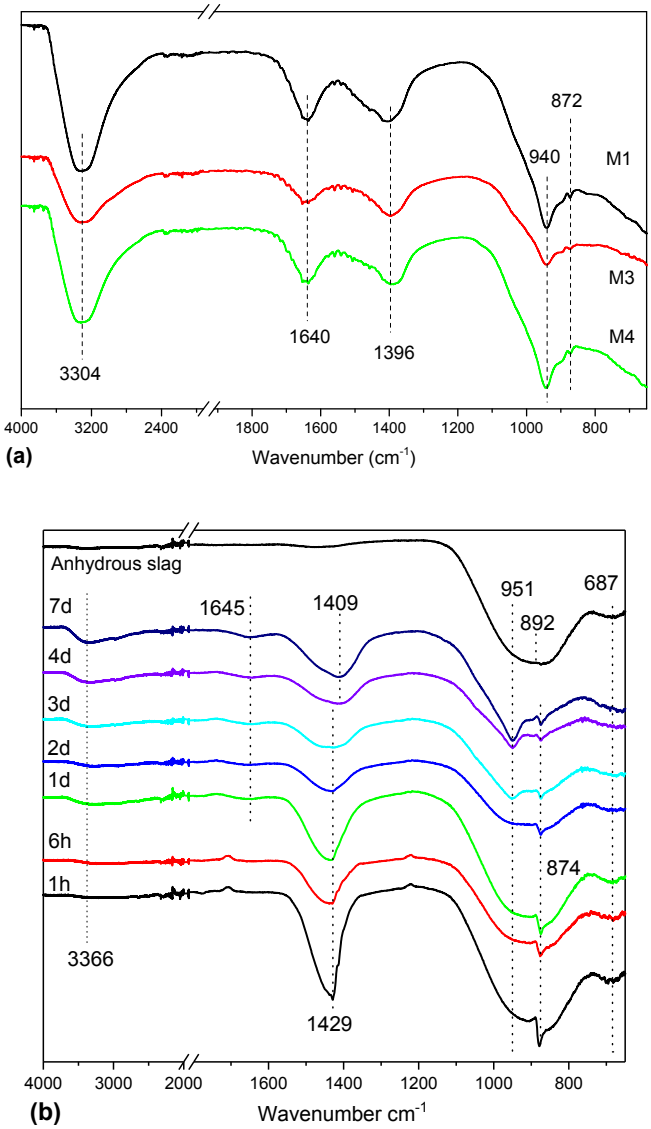

Fig. 4. FTIR spectra of: (a) mixtures at 28 d; (b) M3 at different curing ages.

The infrared spectroscopic results of anhydrous slag and sample M3 at different curing ages are presented in Fig. 4b. The IR spectrum of anhydrous slag contains a distinct intensity band centred at around 892 cm^{-1} (characteristic of T-O, T is Si or Al, bonds of tetrahedral silicates) [11], and another small intense band at approximate 687 cm^{-1} represents the functional group of AlO_2 [33]. After mixing with sodium carbonate solution, two sharp peaks at around 1429 cm^{-1} and 874 cm^{-1} appear in the spectrum of sample after 1 h of casting, which are assigned to the vibration of $v_3[CO_3^{2-}]$ and $v_2[CO_3^{2-}]$, respectively. At the age of 3 d, a new peak centred at 951 cm^{-1} is observed, which is a typical Si–O asymmetric stretching vibration generated by Q^2 units (C-(A)–S–H gel) [34]. After 4 d, the bands centred at approximate 1429 cm^{-1} slightly shift to 1409 cm^{-1}. The small peaks at 1645 cm^{-1} and 3346 cm^{-1} indicate that the samples contain small amount of free water, possibly due to the absorbed free moisture during the sample preparation.

In general, the vibration of CO_3^{2-} groups can be attributed to the used activator, the precipitated $CaCO_3$ or new phases formed during this period. The carbonation or weathering of the samples could also be partly responsible for these bonds. However, these effects are minimized due to the applied preparation process. On the other hand, it is clear the proportions of hump attributed to the gelation start to increase from 3 d after casting.

3.3. XRD

The X-ray diffraction patterns of M3 collected from the alkali-activated slag paste samples at different ages and unreacted GGBS are presented in Fig. 5. Only a broad hump centred at around 30° 2θ is identified for the anhydrous slag, which is attributed to the amorphous phase of short range order of CaO–MgO–Al_2O_3–SiO_2 structure [35–37]. After mixing with sodium carbonate solution, the main reaction products at different ages are slightly different.

At the initial 1 h, the main crystalline binder phases identified in the samples are calcium carbonate calcite ($CaCO_3$, PDF#00-047-1743), aragonite ($CaCO_3$, PDF# 01-071-2392), along with hydrous sodium carbonate: thermonatrite ($Na_2CO_3 \cdot H_2O$, PDF# 00-008-0448) and nahcolite ($NaHCO_3$, PDF# 01-074-1203). Due to the high concentration of CO_3^{2-} provided by the activator, the precipitation of $CaCO_3$ occurs rapidly when the dissolved Ca^{2+} reaches the

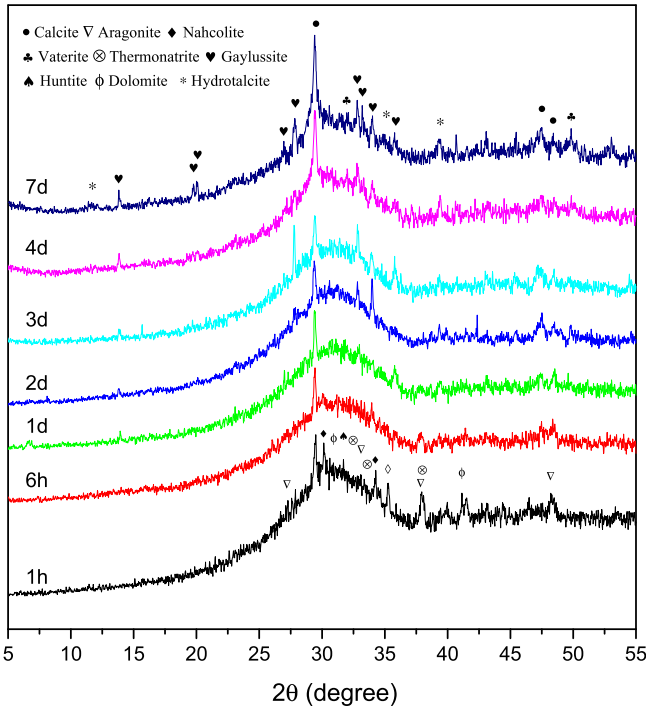

Fig. 5. X-ray diffractograms of anhydrous slag and M3 at different curing ages.

saturation limit. Meanwhile, the formation of huntite ($Mg_3Ca(CO_3)_4$, PDF# 00-014-0409) and dolomite ($MgCa(CO_3)_2$, PDF# 01-075-3699) shows weak reflections, probably due to the raw slag used which contains a high Mg and Fe element (see Table 1).

However, when it comes to 6 h, the crystalline structures detected are weakened and only calcite, aragonite and thermonatrite can be identified. Starting from 1 d after casting, the weak reflections at the positions of 13.9°, 32.8° and 35.8° 2θ indicate the initial formation of gaylussite ($Na_2Ca(CO_3)_2 \cdot 5H_2O$, PDF# 00-021-0343), while the weak reflection at 39.5° 2θ is possibly due to the presence of hydrotalcite ($Mg_{0.667}Al_{0.333}(OH)_2(CO_3)_{0.167} \cdot 0.5H_2O$, PDF# 01-089-0460). A similar XRD pattern is obtained by sample at 2 d after casting but with a slightly intensive reflection of gaylussite. After 3 d of casting, intensive reflections for the formation of calcite, gaylussite and hydrotalcite are identified. For samples at the ages of 4 d and 7 d, the XRD patterns are similar but with higher intensities of the new formed phases. Furthermore, the reflection at 49.8° 2θ is identified as the formation of vaterite ($CaCO_3$, PDF#00-002-0261) at the curing age of 7 d.

As the main crystalline carbonation products, the calcium carbonate calcite, aragonite and vaterite are identified at different ages. There are three crystal polymorphs of $CaCO_3$, namely calcite, aragonite and vaterite, and it is known that the temperature and environmental pH have strong effects on the preference of the $CaCO_3$ polymorphs [38]. The aragonite precipitated at the very early age (about 1 h) is a metastable polymorph of calcium carbonate and gradually transfers to the more stable phase calcite. After 2 d of curing, the reflections of aragonite almost disappear. On the other hand, hydrous sodium carbonates such as nahcolite and thermontrite are observed at the early stages as well. According to the phase diagram of Na_2CO_3–$NaHCO_3$–CO_2–H_2O versus temperature and CO_2 partial pressure [24], the formation of natron and trona should be the main products. However, caused by the samples preparation process (oven dried at 40 °C), these phases are not observed because the decrystallization of natron and trona happens at very low temperature (below 40 °C). Nevertheless, the identified thermonatrite, the recrystallized product of natron at 37–38 °C, indicates the existence of natron ($Na_2CO_3 \cdot 10H_2O$) in the reaction products. Furthermore, the reflections of hydrous sodium carbonates are gradually disappearing till 2 d of casting, indicating the transformation of hydrous sodium carbonates to other new products, i.e. gaylussite and hydrotalicte.

3.4. TG-DTG

The TG-DTG analysis results (M3) heated from 20 to 1000 °C at different ages are shown in Fig. 6a, confirming again different reaction products are formed at the early stages. In general, the mass loss happening below 200 °C is due to the physically bound water or free water evaporation. The peaks on the DTG curves at approximate 491 °C and 614 °C are attributed to the decomposition of carbonate salts. Corresponding to the XRD results, the carbonate salts can be different polymorphs of calcium carbonate, such as aragonite [39] and calcite. Furthermore, due to the activator applied, the mass change at about 903 °C is possibly attributed to the decomposition of sodium carbonate to Na_2O and CO_2 [40]. When the reaction approaches 3 d/4 d, a new decomposition peak centred at around 296 °C is observed that is then slightly shifting to a higher position (326 °C) and the peak at around 537 °C after 7 d of curing indicates the dehydroxylation and decarbonation of hydrotalcite (Fig. 5). It is difficult to distinguish the decarbonation of gaylussite and calcite, however, the small shoulder at around 138 °C shows that dehydration of gaylussite [41]. The shoulder is also observed in the samples after 2 d of curing, which is in line with the XRD results. Moreover, the peaks above 840 °C can be attributed to the decomposition of sodium carbonate, which can be the decomposed reaction product from gaylussite after releasing CO_2 [41]. It should be noted that the mass loss before 200 °C is substantially increased after 3 d of curing, probably due to the formation of C-(A)–S–H gel (Fig. 4).

3.5. SEM

The SEM images of samples M3 at different ages are presented in Fig. 7. As can be seen, the initial dissolution of GGBS, precipitation of calcium carbonate and initial gelation process of reaction products can be clearly observed. At the first 1 h, the dissolution process of slag particles starts when it contacts with the alkali activator. Small grains can be observed on the surface of slag particles (Fig. 7–1 h (a,b)) which gradually become more obvious till 1 d after casting, and this is primarily considered to be the initial precipitation process of calcium carbonate. When it comes to 2 d, corresponding with the reaction kinetics (Fig. 2) and FTIR (Fig. 4) results, the gel-like structures on the surface of slag particles (Fig. 7–2 d(b)) are assigned to the initial formation of C-(A)–S–H gel. Furthermore, an increased denser microstructure of samples from 3 d to 7 d is observed, indicating the ongoing process of gelation. In the meantime, the new phases are generated, as shown in Fig. 7– d(b).

3.6. Compressive strength

The compressive strength of Na_2CO_3 activated slag with different alkali contents and W/S ratios at the curing ages of 7 d, 28 d and 180 d, respectively, are shown in Fig. 8. It is clear that the factors of water to solid ratio, alkali content and curing age have significant effects on the compressive strength. The 7 d, 28 d and 180 d compressive strength of mixtures range from 18 MPa to 39 MPa, 26 MPa–50 MPa and 32 MPa–54 MPa, respectively, which shows that these materials can be applied to construction with different strength class requirements to a large extent.

As can be seen, the compressive strength of samples is proportional to the sodium carbonate content and W/S ratio. Within the range of the factors studied (AC, 3%–5%; W/S, 0.4 to 0.5), the effect of water to solid ratio is considered to be more prominent than that of alkali content. To specify, when the alkali content increases from 3% to 5%, the increase of 7 d compressive strength of samples with a W/S of 0.45 is 41%, while with an alkali content of 4% that of W/S from 0.5 to 0.4 is up to 63%. The reason could be related to the fact that more concentrated alkali solution is more effective in attacking the slag particles and the reaction rate is supposed to be faster (Fig. 2).

The relationship between the sodium carbonate concentration and the compressive strength of the samples at different curing ages is investigated. As shown in Fig. 9, it is obvious that within the investigated range here, the initial alkali concentrations play a dominating role on the mechanical properties. Moreover, an approximately linear relationship is observed for samples at the different ages. The interaction between AC and W/S is also observed to have a certain degree of influences, which means that alkali content will more effectively affect the compressive strength of samples produced with a lower alkali content. For example, from W/S ratios of 0.45 to 0.4 at 7d curing, the average increase of strength of AC 3% samples is 29%, whereas to the AC 5% samples it is only 21%.

3.7. Discussion

Previously, Xu and Provis [23] proposed a mechanism and reported that initially Ca^{2+} dissolves from slags and then forms

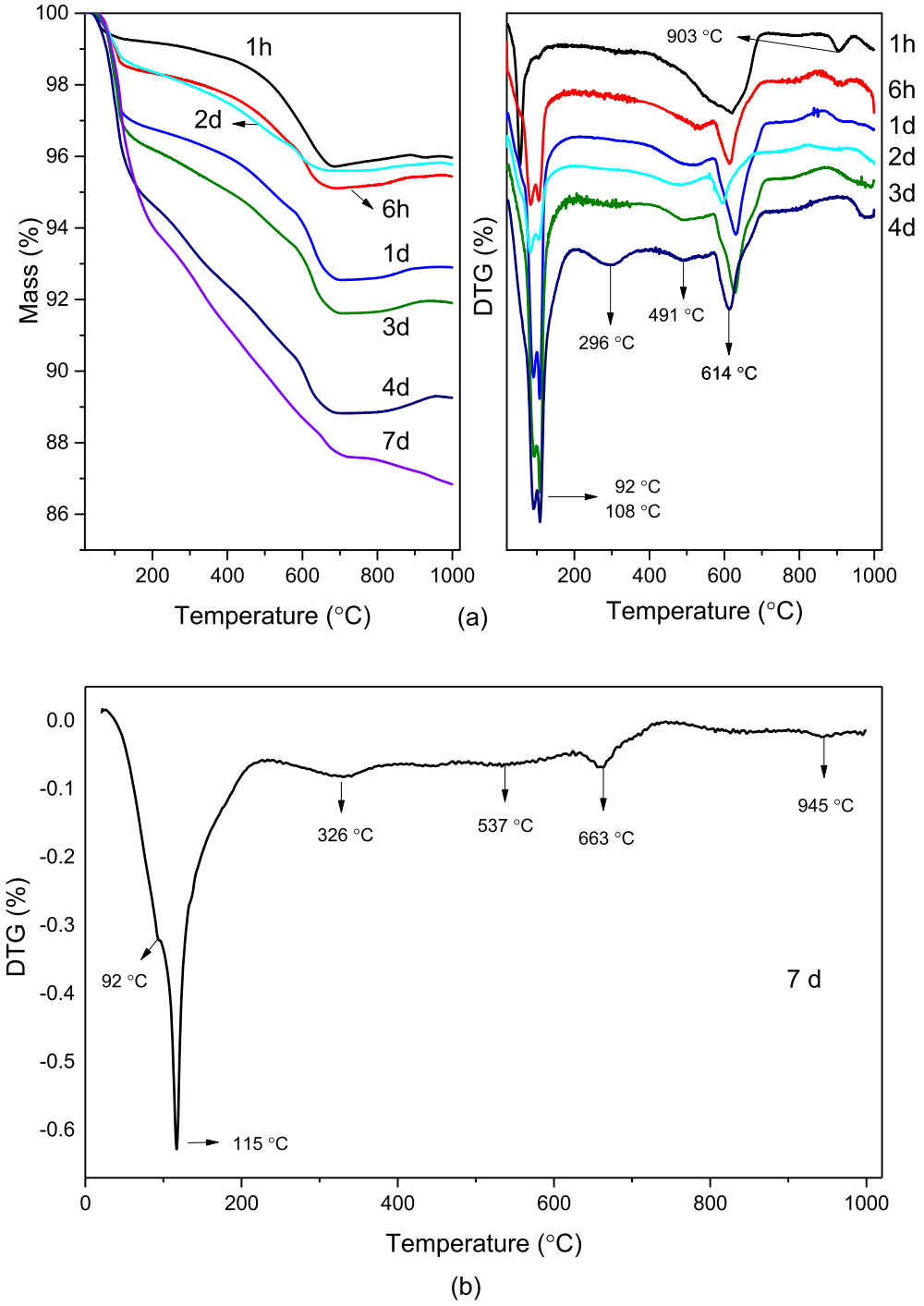

Fig. 6. (a) TG-DTG results of M3 at different curing ages; (b) DTG result of M3 after 7 d of curing.

$CaCO_3$, which will decrease the pH of the system. Then the formation of C–S–H gel will take Ca^{2+} from $CaCO_3$, releasing CO_3^{2-} to participate another cycle of reaction. However, the mechanism proposed is based on the characterization of aged products, which explains the ongoing reaction process of Na_2CO_3 activated GGBFS rather than the initial reaction. Bernal et al. [27] reported a conceptual description of the pore solution chemistry within a sodium carbonate-activated slag binder, however, the reactions happened during the dormant period and the key factors triggering the restarted reaction still require further investigation.

Based on the present results, it is clear that the gelation process of C-(A)–S–H gel started at 2–3 d after casting, confirmed by the FTIR (Fig. 4) and SEM results (Fig. 7). As a result, the phase changes before gelling is of great interest. The precipitation of calcium carbonate is confirmed by the XRD and TG results (Fig. 6a). Bernal et al. [27] proposed that the gaylussite was formed at ~1 d and then started converting to $CaCO_3$ from days 1 to 5–7. In the meantime, the Mg^{2+} dissolved from slag will react with Al forming hydrotalcite. However, different phenomena are observed in the present study. The intensive formation of gaylussite is only observed during the curing along with the generation of hydrotalcite after around 2 d/3 d, which is in line with the TG-DTG results. While at the early

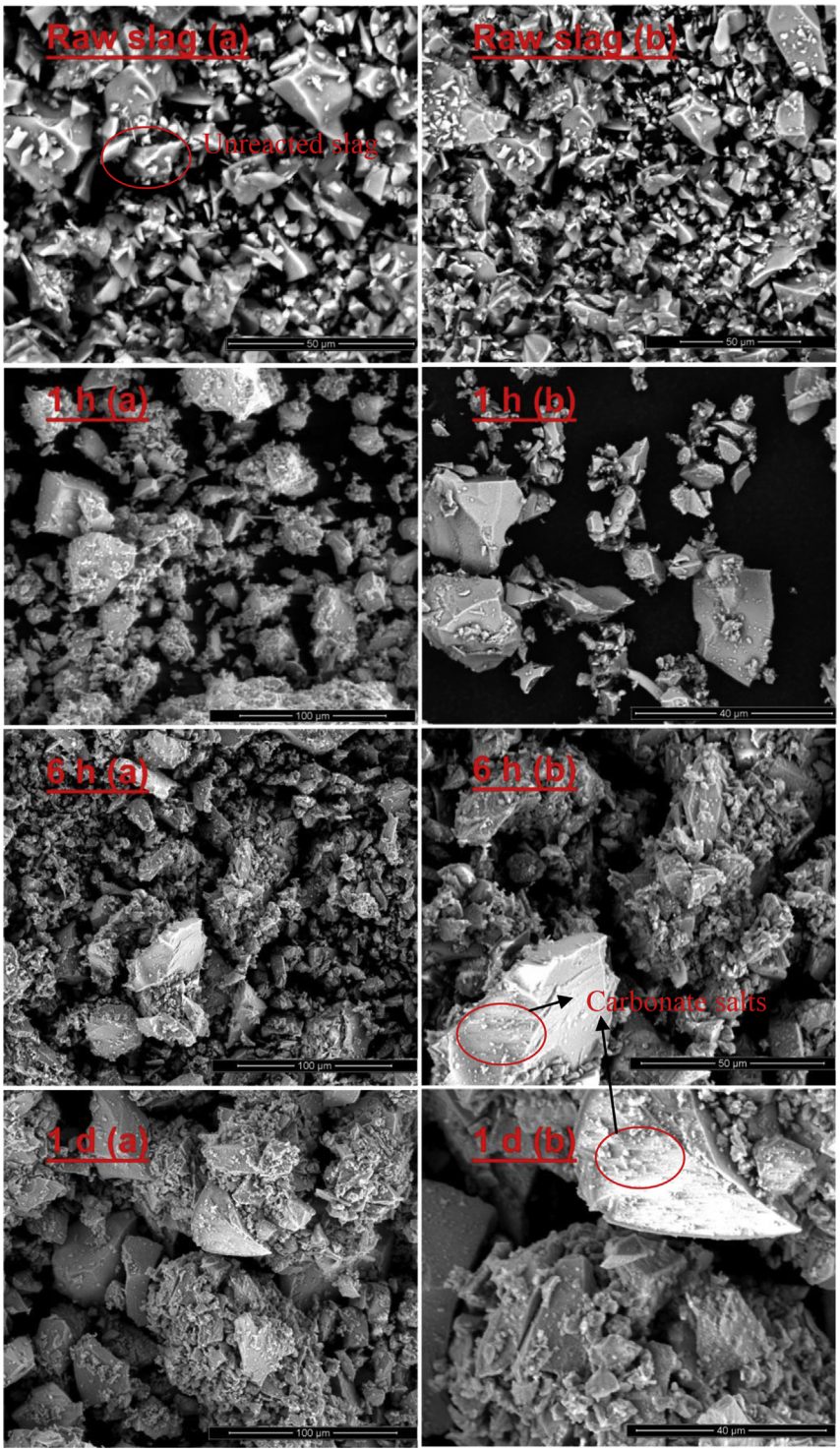

Fig. 7. SEM pictures of anhydrous slag and M3 at the ages of: (a) 1 h-1 d; (b) 2 d-7 d.

age (≤2 d), only the existence of different polymorphs of calcium carbonate, such as aragonite and calcite, and a tiny amount of gaylussite can be clearly identified. It is clear that the CO_3^{2-} concentration in the pore solution controls the reaction of sodium carbonate activated slag due to the low saturation limit of calcium carbonate. In this case, according to the results, it is most likely that the accumulation of gaylussite and formation of hydrotalcite decrease the CO_3^{2-} concentration to a certain level, and then the Ca^{2+} concentration increases, leading to the precipitation of C-(A)–S–H gel.

On the other hand, it has been reported that pH value of solution plays a significant role on the initial dissolution of the precursor and a pH value lower than 9.5 is not sufficient to form the C–S–H gel [17,42]. As a result, changes on pH of sodium carbonate activated slag are worth to be further studied. Because of the lengthened reaction process, the fresh paste remains unhardened after 2 h

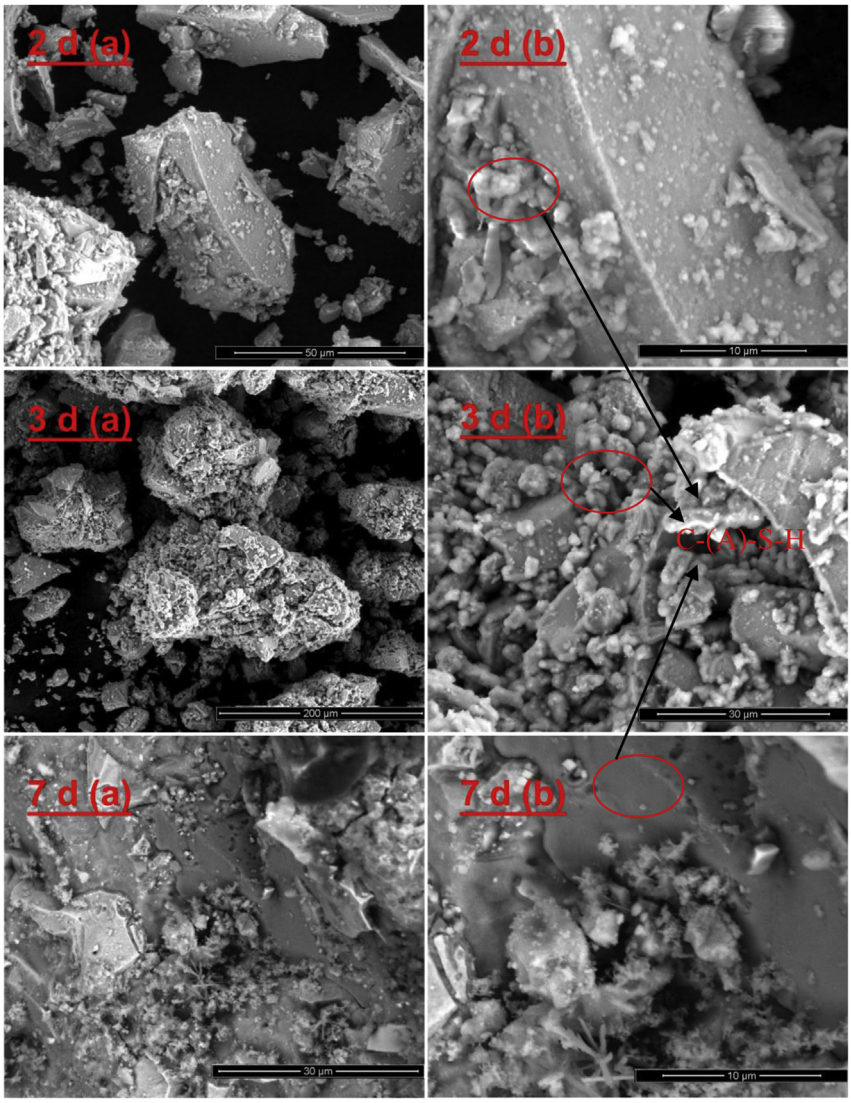

Fig. 7. (*continued*).

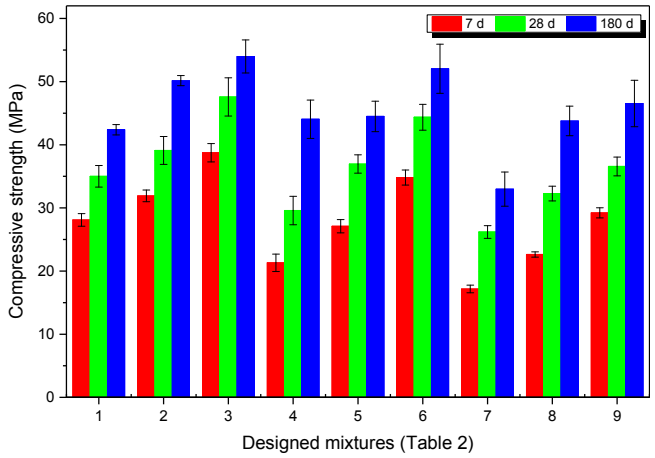

Fig. 8. Effect of alkali content, water to solid ratio and curing age on the compressive strength of Na_2CO_3 activated GGBFS.

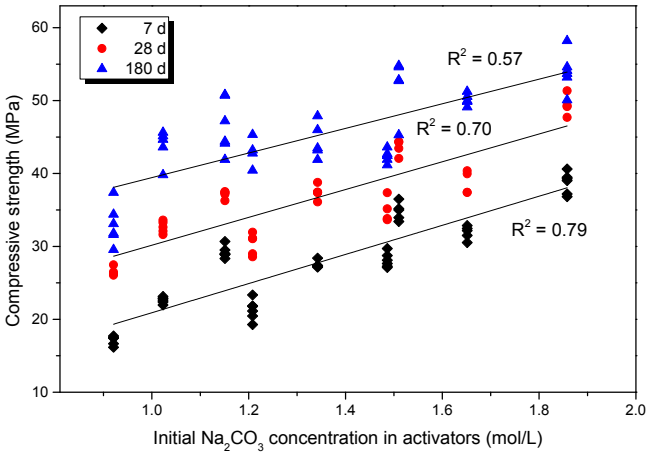

Fig. 9. Relationship between initial alkali concentration and compressive strength of samples at 7 d, 28 d and 180 d, respectively.

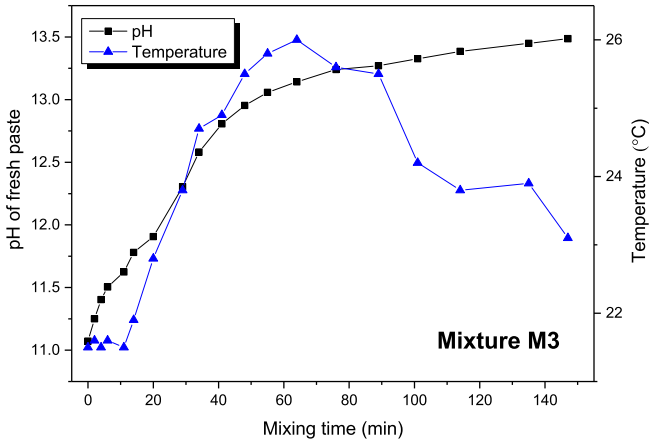

Fig. 10. pH value and temperature changes of Na_2CO_3 activated GGBFS paste during the initial mixing stage.

of mixing, which provides the possibility of measuring its pH changes during the mixing time. By incorporating a pH meter (780 pH Meter, Metrohm) into the fresh paste during the mixing, the pH values of the fresh paste were measured and the results are shown in Fig. 10. As can be seen, the pH value increases firstly dramatically until about 60 min after mixing and then increases slowly till the end of testing. It is clear that the pH of the pore solution is already sufficient to dissolve slag particles at the early stage, releasing ions for the gelation of C-(A)–S–H gel. In this case, the only barrier to the gelation process is the Ca^{2+} concentration that is controlled by the CO_3^{2-} concentration. The results confirm that the accumulation of gaylussite and formation of hydrotalcite play a significant role on decreasing the CO_3^{2-} anions, which then lead to the formation of the strength-giving phases, i.e. C-(A)–S–H gel.

4. Conclusions

This study aims at the time-dependent characterization of GGBFS activated by sodium carbonate. The reaction process and reaction products of $NaCO_3$ activated slag were investigated by employing isothermal calorimetry, FTIR, XRD, TG-DTG and SEM. Furthermore, the influential factors such as the alkali dosages, water to binder ratio and curing age on the mechanical properties were evaluated by a full factorial experiment. The following conclusions can be reached:

- A long dormant period of approximate 40–70 h and a trend of an increasing pH value of the pore solution at the early age is observed.
- The gelation of C-(A)–S–H gel starts approximately 2 d after casting.
- The accumulation of gaylussite and formation of hydrotalcite play a significant role on decreasing CO_3^{2-} anions, which then lead to the formation of C-(A)–S–H gel.
- Water to solid ratio is a determinant factor of the compressive strength.
- A linear relationship between the initial alkali concentration and compressive strength at different ages is derived.

Acknowledgements

This research was carried out under the support of China Scholarship Council (CSC) and the Department of the Built Environment at Eindhoven University of Technology. Furthermore, the authors wish to express their gratitude to the following sponsors of the Building Materials research group at TU Eindhoven: Rijkswaterstaat Grote Projecten en Onderhoud, Graniet-Import Benelux, Kijlstra Betonmortel, Struyk Verwo, Attero, Enci, Rijkswaterstaat Zee en Delta - District Noord, Van Gansewinkel Minerals, BTE, V.d. Bosch Beton, Selor, GMB, Icopal, BN International, Eltomation, Knauf Gips, Hess AAC Systems, Kronos, Joma, CRH Europe Sustainable Concrete Centre, Cement&BetonCentrum, Heros, Inashco, Keim, Sirius International, Boskalis, NNERGY, Tata Steel, Millvision, Sappi, Studio Roex and Van Berlo Groep (in chronological order of joining).

References

[1] S.A. Bernal, R. Mejía, D. Gutiérrez, J.L. Provis, Engineering and durability properties of concretes based on alkali-activated granulated blast furnace slag/metakaolin blends, Constr. Build. Mater 33 (2012) 99–108, http://dx.doi.org/10.1016/j.conbuildmat.2012.01.017.
[2] F. Pacheco-Torgal, Z. Abdollahnejad, A.F. Camoes, M. Jamshidi, Y. Ding, Durability of alkali-activated binders: a clear advantage over Portland cement or an unproven issue? Constr. Build. Mater 30 (2012) 400–405, http://dx.doi.org/10.1016/j.conbuildmat.2011.12.017.
[3] B. Yuan, C. Straub, S. Segers, Q.L. Yu, H.J. Brouwers, Sodium carbonate activated slag as cement replacement in autoclaved aerated concrete, Ceram. Int. 43 (2017) 6039–6047, http://dx.doi.org/10.1016/j.ceramint.2017.01.144.
[4] D.M.A. Huiskes, A. Keulen, Q.L. Yu, H.J.H. Brouwers, Design and performance evaluation of ultra-lightweight geopolymer concrete, Mater. Des. 89 (2015) 516–526, http://dx.doi.org/10.1016/j.matdes.2015.09.167.
[5] I.G. Richardson, A.R. Brough, G.W. Groves, C.M. Dobson, The characterization of hardened alkali-activated blast-furnace slag pastes and the nature of the calcium silicate hydrate (C-S-H) phase, Cem. Concr. Res. 24 (1994) 813–829.
[6] X. Gao, Q.L. Yu, H.J.H. Brouwers, Properties of alkali activated slag–fly ash blends with limestone addition, Cem. Concr. Compos 59 (2015) 119–128, http://dx.doi.org/10.1016/j.cemconcomp.2015.01.007.
[7] X. Gao, Q.L.L. Yu, H.J.H.J.H. Brouwers, Reaction kinetics, gel character and strength of ambient temperature cured alkali activated slag–fly ash blends, Constr. Build. Mater 80 (2015) 105–115, http://dx.doi.org/10.1016/j.conbuildmat.2015.01.065.
[8] A.R. Brough, A. Atkinson, Sodium silicate-based, alkali-activated slag mortars Part I. strength, hydration and microstructure, Cem. Concr. Res. 32 (2002) 865–879.
[9] D.M. Roy, W. Jiang, M.R. Silsbee, Chloride diffusion in ordinary, blended, and alkali-activated cement pastes and its relation to other properties, Cem. Concr. Compos 30 (2001).
[10] T. Bakharev, J.G. Sanjayan, Y.B. Cheng, Sulfate attack on alkali-activated slag concrete, Cem. Concr. Res. 32 (2002) 211–216, http://dx.doi.org/10.1016/S0008-8846(01)00659-7.
[11] S.A. Bernal, E.D. Rodriguez, R. Mejia de Gutierrez, J.L. Provis, S. Delvasto, Activation of metakaolin/slag blends using alkaline solutions based on chemically modified silica fume and rice husk ash, Waste Biomass Valorizatio 3 (2011) 99–108, http://dx.doi.org/10.1007/s12649-011-9093-3.
[12] S. Wang, K.L. Scrivener, P.L. Pratt, Factors affecting the strength of alkali-activated slag, Cem. Concr. Res. 24 (1994) 1033–1043.
[13] T. Bakharev, J.G. Sanjayan, Y.B. Cheng, Alkali activation of Australian slag cements, Cem. Concr. Res. 29 (1999) 113–120, http://dx.doi.org/10.1016/S0008-8846(98)00170-7.
[14] A.R. Brough, M. Holloway, J. Sykes, A. Atkinson, Sodium silicate-based alkali-activated slag mortars Part II. the retarding effect of additions of sodium chloride or malic acid, Cem. Concr. Res. 30 (2000) 1375–1379.
[15] A.M. Rashad, A comprehensive overview about the influence of different additives on the properties of alkali-activated slag – a guide for civil engineer, Constr. Build. Mater 47 (2013) 29–55, http://dx.doi.org/10.1016/j.conbuildmat.2013.04.011.
[16] D.M. Roy, Alkali-activated cements opportunities and challenges, Cem. Concr. Res. 29 (1999) 249–254, http://dx.doi.org/10.1016/S0008-8846(98)00093-3.
[17] V. Zivica, Effects of type and dosage of alkaline activator and temperature on the properties of alkali-activated slag mixtures, Constr. Build. Mater 21 (2007) 1463–1469, http://dx.doi.org/10.1016/j.conbuildmat.2006.07.002.
[18] A.F. Jimenez, F. Puertas, Setting of alkali-activated slag cement. influence of activator nature, Adv. Cem. Res. 13 (2001) 115–121, http://dx.doi.org/10.1680/adcr.2001.13.3.115.
[19] J.G. Sanjayan, F. Collins, Microcracking and strength development of alkali activated slag concrete, Cem. Concr. Compos 23 (2001) 345–352.
[20] F. Collins, J.G. Sanjayan, Cracking tendency of alkali-activated slag concrete subjected to restrained shrinkage, Cem. Concr. Res. 30 (2000) 791–798, http://dx.doi.org/10.1016/S0008-8846(00)00243-X.
[21] C. Duran Atis, C. Bilim, O. Celik, O. Karahan, Influence of activator on the strength and drying shrinkage of alkali-activated slag mortar, Constr. Build. Mater 23 (2009) 548–555, http://dx.doi.org/10.1016/j.conbuildmat.2007.10.011.
[22] X. Gao, Q.L. Yu, H.J.H. Brouwers, Assessing the porosity and shrinkage of alkali activated slag-fly ash composites designed applying a packing model, Constr.

Build. Mater 119 (2016) 175–184, http://dx.doi.org/10.1016/j.conbuildmat.2016.05.026.
[23] H. Xu, J.L. Provis, J.S.J. Van Deventer, P.V. Krivenko, Characterization of Aged slag concretes, Mater. J. 105 (2008) 131–139.
[24] S.A. Bernal, J.L. Provis, D.G. Brice, A. Kilcullen, P. Duxson, J.S.J. van Deventer, Accelerated carbonation testing of alkali-activated binders significantly underestimates service life: the role of pore solution chemistry, Cem. Concr. Res. 42 (2012) 1317–1326, http://dx.doi.org/10.1016/j.cemconres.2012.07.002.
[25] S.A. Bernal, R. San Nicolas, J.L. Provis, R. Mejia de Gutierrez, J.S.J. van Deventer, Natural carbonation of aged alkali-activated slag concretes, Mater. Struct. 47 (2013) 693–707, http://dx.doi.org/10.1617/s11527-013-0089-2.
[26] T.C. Alex, A.M. Kalinkin, S.K. Nath, B.I. Gurevich, E.V. Kalinkina, V.V. Tyukavkina, S. Kumar, Utilization of zinc slag through geopolymerization: influence of milling atmosphere, Int. J. Min. Process 123 (2013) 102–107, http://dx.doi.org/10.1016/j.minpro.2013.06.001.
[27] S.A. Bernal, J.L. Provis, R.J. Myers, R. San Nicolas, J.S.J. van Deventer, Role of carbonates in the chemical evolution of sodium carbonate-activated slag binders, Mater. Struct. 48 (2014) 517–529, http://dx.doi.org/10.1617/s11527-014-0412-6.
[28] B. Yuan, Q.L. Yu, H.J.H. Brouwers, Evaluation of slag characteristics on the reaction kinetics and mechanical properties of Na_2CO_3 activated slag, Constr. Build. Mater 131 (2017) 334–346, http://dx.doi.org/10.1016/j.conbuildmat.2016.11.074.
[29] S.A. Bernal, R.S. Nicolas, R.J. Myers, R. Mejia De Gutierrez, F. Puertas, J.S.J. Van Deventer, J.L. Provis, MgO content of slag controls phase evolution and structural changes induced by accelerated carbonation in alkali-activated binders, Cem. Concr. Res. 57 (2014) 33–43, http://dx.doi.org/10.1016/j.cemconres.2013.12.003.
[30] C. Shi, R.L. Day, A calorimetric study of early hydration of alkali-slag cements, Cem. Concr. Res. 25 (1995) 1333–1346.
[31] X. Ke, S.A. Bernal, J.L. Provis, Controlling the reaction kinetics of sodium carbonate-activated slag cements using calcined layered double hydroxides, Cem. Concr. Res. 81 (2016) 24–37, http://dx.doi.org/10.1016/j.cemconres.2015.11.012.
[32] D. Ravikumar, N. Neithalath, Reaction kinetics in sodium silicate powder and liquid activated slag binders evaluated using isothermal calorimetry, Thermochim. Acta 546 (2012) 32–43, http://dx.doi.org/10.1016/j.tca.2012.07.010.
[33] K. Komnitsas, D. Zaharaki, V. Perdikatsis, Effect of synthesis parameters on the compressive strength of low-calcium ferronickel slag inorganic polymers, J. Hazard. Mater 161 (2009) 760–768, http://dx.doi.org/10.1016/j.jhazmat.2008.04.055.
[34] I. Garcia Lodeiro, D.E. Macphee, A. Palomo, A.J. Fernandez, Effect of alkalis on fresh C–S–H gels. FTIR analysis, Cem. Concr. Res. 39 (2009) 147–153, http://dx.doi.org/10.1016/j.cemconres.2009.01.003.
[35] M.B. Haha, G.L. Saout, F. Winnefeld, B. Lothenbach, Influence of activator type on hydration kinetics, hydrate assemblage and microstructural development of alkali activated blast-furnace slags, Cem. Concr. Res. 41 (2011) 301–310, http://dx.doi.org/10.1016/j.cemconres.2010.11.016.
[36] M.O. Yusuf, M.A. Megat Johari, Z.A. Ahmad, M. Maslehuddin, Strength and microstructure of alkali-activated binary blended binder containing palm oil fuel ash and ground blast-furnace slag, Constr. Build. Mater 52 (2014) 504–510, http://dx.doi.org/10.1016/j.conbuildmat.2013.11.012.
[37] S. Wang, K.L. Scrivener, Hydration products of alkali activated slag cement, Cem. Concr. Res. 25 (1995) 561–571, http://dx.doi.org/10.1016/0008-8846(95)00045-E.
[38] Y. Sheng Han, G. Hadiko, M. Fuji, M. Takahashi, Crystallization and transformation of vaterite at controlled pH, J. Cryst. Growth 289 (2006) 269–274, http://dx.doi.org/10.1016/j.jcrysgro.2005.11.011.
[39] S. Yoshioka, Y. Kitano, Transformation of aragonite to calcite through heating, Geochem. J. 19 (1985) 245–249.
[40] J.W. Kim, H.G. Lee, Thermal and carbothermic decomposition of Na_2CO_3 and Li_2CO_3, Metall. Mater. Trans. B 32 (2001) 17–24, http://dx.doi.org/10.1007/s11663-001-0003-0.
[41] D.R. Jornson, W.A. Ross, Gaylussite: thermal properties by simultaneous thermal analysis, Am. Mineral. 58 (1973) 778–784.
[42] S. Song, H.M. Jennings, Pore solution chemistry of alkali-activated ground granulated blast-furance slag, Cem. Concr. Res. 29 (1999) 159–170.